Scientific Research Publishing

Materials Sciences and Applications, 2018, 9, 228-245
http://www.scirp.org/journal/msa
ISSN Online: 2153-1188
ISSN Print: 2153-117X

Influence of MIG/MAG Welding Process on Mechanical and Pitting Corrosion Behaviors on the Super-Duplex Stainless Steel SAF 2507 Welded Joints

Bruno Leonardy S. Lopes[1], Samuel F. Rodrigues[1], Eden S. Silva[1,2], Gedeon S. Reis[1], Waldemir dos P. Martins[1], Juvenilson Costa Damascena[1], Valdemar S. Leal[1]

[1]Graduate Program in Materials Engineering, Federal Institute of Education, Science and Technology of Maranhão—IFMA, São Luís, MA, Brazil
[2]Engineering Coordination, Universidade UNICEUMA, São Luís, MA, Brazil
Email: samuel.filgueiras@ifma.edu.br

How to cite this paper: Lopes, B.L.S., Rodrigues, S.F., Silva, E.S., Reis, G.S., Martins, W. dos P., Damascena, J.C. and Leal, V.S. (2018) Influence of MIG/MAG Welding Process on Mechanical and Pitting Corrosion Behaviors on the Super-Duplex Stainless Steel SAF 2507 Welded Joints. *Materials Sciences and Applications*, **9**, 228-245.
https://doi.org/10.4236/msa.2018.92015

Received: October 18, 2017
Accepted: February 2, 2018
Published: February 5, 2018

Abstract

The main objective of this research is to better understand the correlation between the constituent phases presented in the super-duplex steel SAF 2507 when it is under welding process by arc shielding gas MIG-MAG (Metal Inert Gas-Metal Active Gas). Conventional short circuit transfer and derivative STT (Surface Tension Transfer) using the 2594 welding wire as a filler metal and the effects on welding power in hardness, toughness and pitting corrosion are considered here. The results showed that the welding energy (Ew) changed the α/γ-phase's balance and occasionally formed σ-phase in ferrite grain boundaries which led to changes in hardness, toughness and pitting corrosion resistance in molten zone (MZ), heat activated zone (HAZ) and metal base regions (MB). Furthermore, the increased amount of γ-phase improved the pitting corrosion resistance index (PRENγ) mainly in the MZ. This is due to decrease of α-phase fraction and formation of coarser grains, for higher welding energy. The toughness in the MZ decreased with less formation of γ-phase, coalescence of ferritic grains and localized formation of σ-phase, raising the hardness in the HAZ when the welding energy was lower.

Keywords

Super-Duplex Steels, Welding, Toughness, Pitting Corrosion, Microhardness

1. Introduction

The development of alloys means major advances in the manufacture of high

strength materials with adequate corrosion resistance and good weldability. Stainless steels are part of this kind of alloys in which when are exposed to an atmosphere containing oxygen a preventive passive oxide layer is formed in order to protect the metal from an aggressive environment [1] [2].

Stainless super-duplex steels (SSDS) are alloys of the type Fe-Cr-Ni-Mo-N, and are used in a wide variety of applications, such as chemical, petrochemical, oil and gas industrial plants, manufacturing of tubular products and offshore structural industries [3] [4]. The application of these alloys has also been justified due to the recent discovering of oil and gas reserves in the pre-salt layer. Thus, the use of materials with high performance against wear and pitting is required [5] [6] [7] [8].

Welding is one of the most important and versatile manufacturing facilities available in the industry. Welding is used to join hundreds of different commercial alloys into many different forms. More than 50% of all stainless steel delivered to the world has undergone some welding process [6]. In this way, the application of this material which presents excellent mechanical and corrosion properties is essential.

Studies in the literature have been reported in order to better understand the mechanical and corrosive mechanisms that outline the preferential formation of the phases present in alloys with function of welding power, microstructural balance and intermetallic phases presented in the molten zone (MZ), heat-activated zone (HAZ) and metal base regions (MB) [7]. These studies also include the relationship between the welding processes and its influence on the phases formed with the mechanisms of strength as well as its responses to the corrosion susceptibility and anomalies that can promote equipment failure without notice during operation [8] [9].

2. Background

The super-duplex steels are a family of steels which contain approximately equal fractions of ferrite (α) and austenite (γ) phases, 50/50 by volume [10] [11]. This microstructure can be achieved by balancing the alloying elements, heat treatment and/or thermomechanical processes. The change in the balance of phases during the welding process can induce changes in the material mechanical properties with the possible formation of intermetallic compounds [12] [13].

The ferrite phase is stable and rich in chromium and molybdenum and presents excellent mechanical properties (e.g. high yield strength) due to the fine grain size of the microstructure, which is dependent on the welding process [11]. However, the austenite phase is stable and has higher concentration of nickel, manganese and nitrogen, with high toughness and ductility. Some of these elements, which are added as an alloying element in austenite, can precipitate and lead to pitting corrosion [13] [14].

Considering the aspects of the ferrite and the austenite phases regarding their resistance to pitting corrosion, results in the literature have shown that better re-

sistance to corrosion is attained when these phases are presented together, such as in super-duplex stainless steels [12]. On the other hand, they may be more susceptible to localized corrosion, such as pites [13] [14]. What characterizes the resistance to pitting corrosion is the capability of a metal to passivate, form a continuous film and adherent of oxides able to prevent the penetration of oxygen into the matrix [15]. This corrosive process is known as an extremely localized attack, initiated by the breakage of the passive film in regions that presents defects such as inclusions, dislocations, grain boundaries or interfaces [15]. The alloying elements that dictate the resistance to pitting corrosion and the formation of the passivating layer in a stainless steel are Cr, Mo and N [14].

During the welding process, it is difficult to keep the ferrite and austenite phases at a constant 50/50 ratio. One challenge during the welding process is how keep the excellence of the corrosion resistance in the MZ and HAZ. The energy required to melt the metal base with the added metal is generated by the electric arc following the parameters represented shown in Equation (1) (Welding energy, kJ/mm).

$$E = \left(\eta \cdot U \cdot i\right) / v_s \,. \tag{1}$$

where η is the process thermal efficiency, i is the current transferred, U is the applied voltage and v_s the welding speed [16] [17].

The pitting corrosion resistance in stainless steels has been calculated according to the PREN (pitting resistance equivalent numbers) following the ASTM standard A890/A890M, an empirical measurement procedure reported in the literature as a function of the composition of certain elements (Cr, Mo, Mn and N) present in the alloy, according to Equation (2) [16] [17].

$$\text{PREN} = [\%\text{Cr}] + 3.3[\%\text{Mo}] + \xi[\%\text{N}] - [\%\text{Mn}]. \tag{2}$$

where the parameter $16 < \xi < 30$ [17] [18]. From this empirical value, it is possible to measure the resistance to pitting corrosion of the phases and improve the balance α/γ [19] [20]. The super-duplex steels are distinguished for having a value of PREN greater than 40. But there are some issues unclear, such as the fact that the onset of pitting corrosion is not characterized in conditions of low concentrations of the phases, and the PREN differs within the alloy due to these constituents.

This research aims to clarify the correlation between the phases presented in the super-duplex steel SAF 2507, specifically in the MZ-HAZ-MB regions of a welded joint under the arc shielding gas MIG-MAG welding process, while considering the effects of welding energy on hardness, toughness and pitting corrosion.

3. Materials and Methods

The investigated material in this research is the super-duplex steel SAF 2507. The added metal was the welding wire 2594, this wire has been chosen because it presents similar chemical compositions and affordable cost, provided by

NOVAMETAL of Brazil LTDA, in the shape of plates with dimensions of 200 × 200 × 6.0 mm. The chemical composition of both materials is shown in Table 1. According to the literature, SAF 2507 steel exhibits good mechanical properties, such as yield strength (~566 MPa), tensile strength (~836 MPa), maximum elongation of 25%, and high hardness of the phases present, ~286 HV for α-phase and ~272 HV for γ-phase [21] [22].

To identify the phases present in the material when it was submitted to different welding energies, the steel was analyzed by X-ray diffraction in the diffractometer model X-Pert PRO, with copper radiation (CuKα1) and wave length of 1.5406 Å. Phase diagram calculation also was performed using FSSTeel database in the FactSage software in order to estimate the phases present in the alloy.

For microstructural analysis, samples were hot mounted and then polished using silicon carbide papers with grits of 400, 600, 800, 1000 and 1200 that were lubricated with water. Diamond paste (3 μm and 1 μm) was used for fine and final polishing. To analyze the grain boundaries and phases presented, samples were electrolytically etched using 10% oxalic acid solution, and for differentiation of the phases presented, a modified Behara solution was used to etch the steel surface. The microstructural analysis was carried out using an Olympus BX51M optical microscopy and both Image and the MagniSci software to measure the ferrite volume fractions. For this purpose, the austenite areas were subtracted from the total area of each image to provide ferrite volume fraction. For each measurement, 10 to 15 images were taken. A scanning electron microscope Phenom word Pro-X model was used for further investigations.

The welding was carried out following the MIG-MAG process with conventional short circuit transfer and STT (Surface tension transfer). As added metal, welding wire of the type 2594 and Argon shielding gas (Ar + 2% O_2) on a V-shaped welded joint configuration were utilized. Welding procedures took place with the aid of a PW-455m/STT source connected to an HP-20 robotic arm for automatic displacement of the welding torch and temperature range of 40˚C. In order to avoid phase instability as well as the appearance of precipitates, three welding energy values were chosen: EJ1 = 0.607 kJ/mm, EJ2 = 0.633 kJ/mm, and EJ3 = 0.427 kJ/mm, with the current ranging from 85 to 120 A, and voltage between 14.6 and 17.3 V. Furthermore, these energy values were used in order to avoid small variations in the welding energy (Es) which could lead to considerable changes into the α/γ-phase balance. The procedures were performed by an automated process with greater control on the temperature interpasses (average Tp = 40˚C) without excessive energy variations (heat) during welding.

Table 1. Chemical composition of the super-duplex steel SAF 2507 and added metal (% mass). Fe (Balanced).

Material	Cr	Mo	Ni	C	Mn	Si	N	Si
Steel	24.95	3.79	6.91	0.015	0.43	0.26	0.26	0.001
Wire	24.92	3.9	9.19	0.011	0.6	0.46	0.28	0.005

After the welding procedures, the samples were cut in the longitudinal direction for microhardness measurements. These tests were done in a hardness machine model Galileo D200. The micro-hardness (Hv) was mapped according to measurement on the three-phase regions MZ-HAZ-MB under equidistant points in every 0.25 mm from the center of the MZ. In total, three columns with ten different points were measured, starting at the MZ and extending to the MB.

Charpy tests were performed by following the ASTM-E 23 standard specifications on samples with dimensions of 5 × 5 × 55 mm [23]. This was conducted in a testing machine of a model Tinius Olsen LT 032. The temperatures varied from −40˚C to room temperature on the MZ-HAZ-MB region of the three specimens for each condition, named as Joint 1STT-conventional (J1), joint 2STT-conventional (J2) and Joint 3STT-conventional (J3). The pitting corrosion tests were performed according to ASTM G 48 A [24] methodology, which enables to evaluating the weight loss of the steel by immersion in a solution of ferritic chloride ($FeCl_3$) at a temperature of 22˚C [25].

4. Results and Discussions

4.1. Post-Weld Microstructural Aspects

The three joints microstructures with different welding energies on the MZ are shown in Figure 1. Note that there are formations of epitaxial grains as Widmanstätten austenite type needles that grow into the ferritic grains form fine equiaxed grains. There is also the formation of allotriomorphic structures in the ferrite grain boundaries. On the other hand, in the HAZ there is the formation of a columnar mixed microstructure near the MZ with the development of ferrite grains. This is due to the heating affect above the recrystallization temperature and increasing with migration of grain boundaries plus apparently reduction in mechanical strength by heating effects involved in the process.

Note that grain formation is limited and grain growth occurs in MB with morphological variation at different points in the MZ-HAZ regions on the welded joint. These lead to local variations in the micro-structure, potentially affecting the hardness and toughness of the welded region. Differences in the

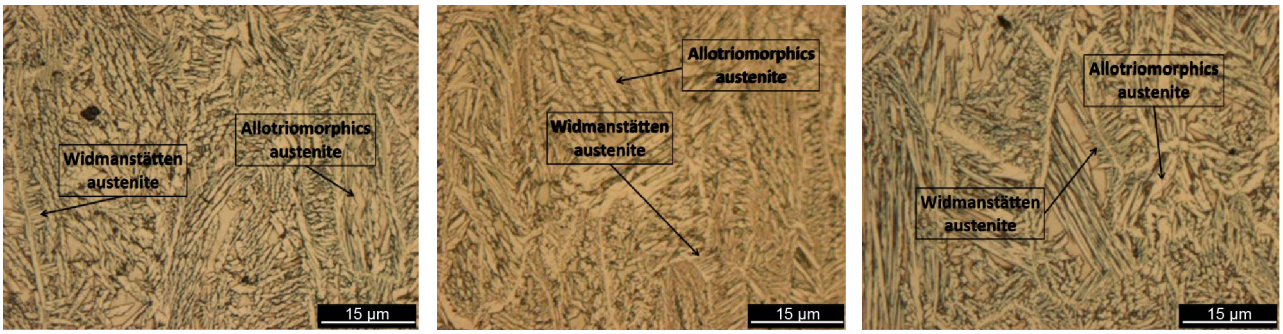

(a) (b) (c)

Figure 1. Configuration of the welded joint on the super-duplex steel SAF 2507 under different welding energies applied: (a) J1 (EJ1 = 0.607 kJ/mm); (b) J2 (EJ2 = 0.633 kJ/mm) and (c) J3 (EJ1 = 0.427 kJ/mm).

shapes of the grains formed between MZ and HAZ interface can also be seen. Taking into account the quantity of each phase, the amount of austenite inside the three regions is higher than ferrite, with the coarser grains of ferrite in the MZ due to higher welding energy. This means that increasing the welding energy, the total volume fraction of ferrite can decreases accompanied with grains coarsening of this phase in the MZ. Furthermore, it appears that the volume fraction of austenite is lower in MZ region than that HAZ and MB regions.

EDS analysis points that the Cr and Mo content in the austenite phase decrease, while amount of Ni increases, as shown in **Figure 2**. Related to HAZ region, a reduction in the concentration of austenite is remarked for a lower welding energy, which is accompanied with an increase in ferrite concentration and grain size.

The microstructures characteristics of the joints J1, J2 and J3 in the MZ as well as the transient phase regions of the joints between the MZ-HAZ-MB are presented in **Figure 3**. The presence of γ-phase (light phase) and α-phase (dark phase) with different morphologies can be seen: intergranular austenite, allotriomorphic austenite on ferrite grain boundaries and Widmanstätten austenite in ferrite grain boundaries growing along the matrix planes in the format of parallel "platelets". Note that higher welding energy and lower interpass temperature results in a lower amount of intergranular austenite and higher amount of Widmanstätten austenite. These are decisive factors for microstructural balance between the α/γ-phases [26] [27] [28] [29].

The calculated volume fractions of the phases in the MZ of the J1 joint was 38% ferrite and 62% austenite, with the higher concentration of Widmanstätten austenite forming in the ferrite grain boundaries, in J2, 37% ferrite and 63% austenite and for J3, 44% ferrite and 56% austenite, the last joint showing higher balance between the phases, with an error of 5%. In solidification of super-duplex stainless steel, the low heat input associated with high cooling rate

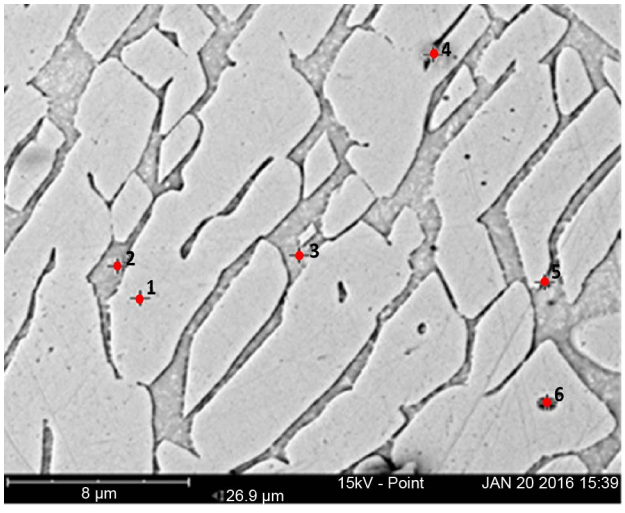

1	Weight percentage	Certainty
Fe	57.7%	99.0%
Cr	22.8%	98.7%
Ni	8.5%	96.3%
N	6.4%	92.8%
Mo	2.4%	95.6%
Mn	1.2%	89.5%
W	1.1%	76.2%

2	Weight percentage	Certainty
Fe	60.1%	99.0%
Cr	20.0%	98.6%
Ni	9.1%	96.5%
N	6.6%	93.4%
Mo	2.0%	95.2%
Mn	1.4%	90.9%
W	0.7%	65.4%

3	Weight percentage	Certainty
Fe	63.0%	99.1%
Cr	18.5%	98.6%
Ni	8.0%	96.1%
N	6.9%	93.6%
Mo	1.6%	94.0%
Mn	1.2%	89.3%
W	0.9%	68.3%

4	Weight percentage	Certainty
Fe	62.6%	99.1%
Cr	16.6%	98.5%
Ni	9.4%	96.7%
N	6.1%	93.1%
Mo	2.2%	94.0%
Mn	1.6%	83.3%
W	1.5%	93.7%

5	Weight percentage	Certainty
Fe	58.9%	99.0%
Cr	21.3%	98.6%
Ni	8.2%	96.2%
N	6.9%	93.2%
Mo	3.0%	96.5%
Mn	1.1%	88.2%
W	0.7%	63.4%

6	Weight percentage	Certainty
Fe	58.3%	99.0%
Cr	23.5%	98.8%
Ni	8.0%	96.2%
N	5.8%	92.5%
Mo	2.2%	95.4%
Mn	1.3%	87.3%
W	0.8%	68.1%

Figure 2. EDS analysis of the MZ (Center of the welding) region that underwent the three welding energies. The presence of Cr, N and Mo and reduced amount of Ni is seen.

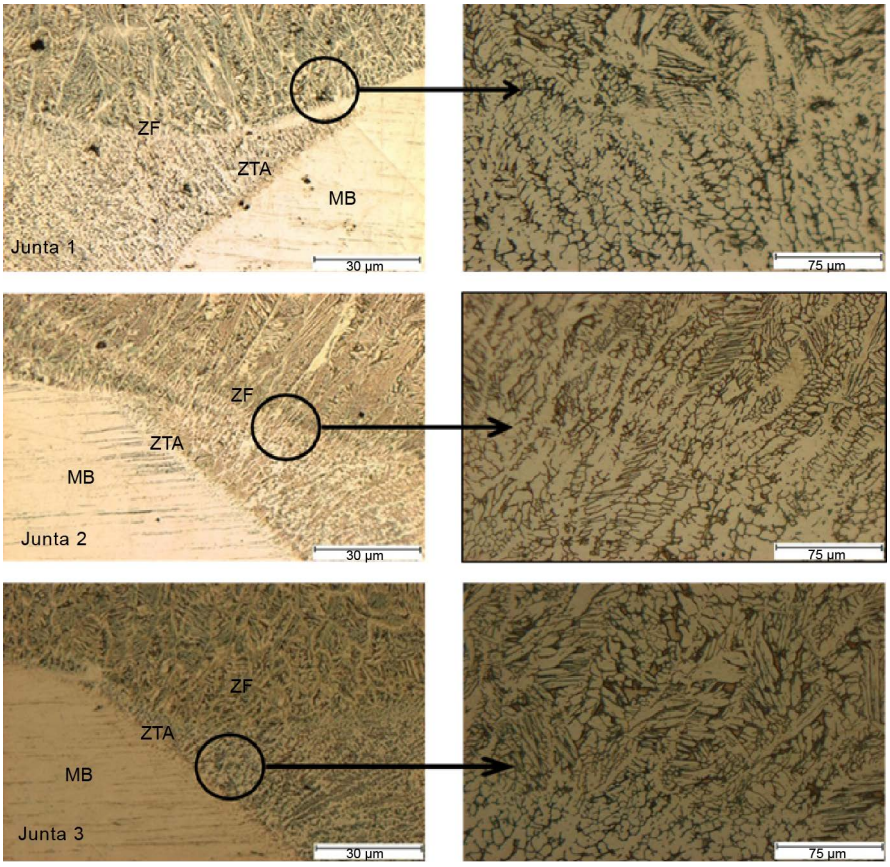

Figure 3. Microstructure of the steel on the three welded joints on the final region of the weld bead region, MZ of (a) J1, (b) J2 and (c) J3.

leads to form a microstructure with a higher volume fraction of ferrite than austenite. On the other hand, the high heat input with low cooling rate produces a higher volume fraction of austenite than ferrite. The small volume fraction of ferrite presented here should be from inhibiting ferrite to austenite transformation due to this last condition.

As can be seen in **Figure 4**, the X-ray diffraction patterns shows the presence of phases α/γ phases, with reduced intensity of the γ-phase and a decrease indication of the rate of phase transformation α/γ as welding energy increases. This analysis also shows that the coarse structures formed near to the MZ is of the α-phase type ($z = 2$ BCC), identified in both MZ and HAZ in smaller quantities than of the γ-phase type ($z = 4$, FCC) in all joints.

4.2. Toughness Tests

The Charpy impact tests applied on the samples are depicted in **Figure 5**. The tests were performed at temperatures of −40˚C and 25˚C. The absorbed energy was higher in the HAZ region than in either the MZ or MB region in the three joints. This indicates good toughness of the welded joints. Regarding the higher quantity of energy absorbed in the HAZ related to MZ, when the value of welding energy applied was higher, there was formation of thin grains of α-phase

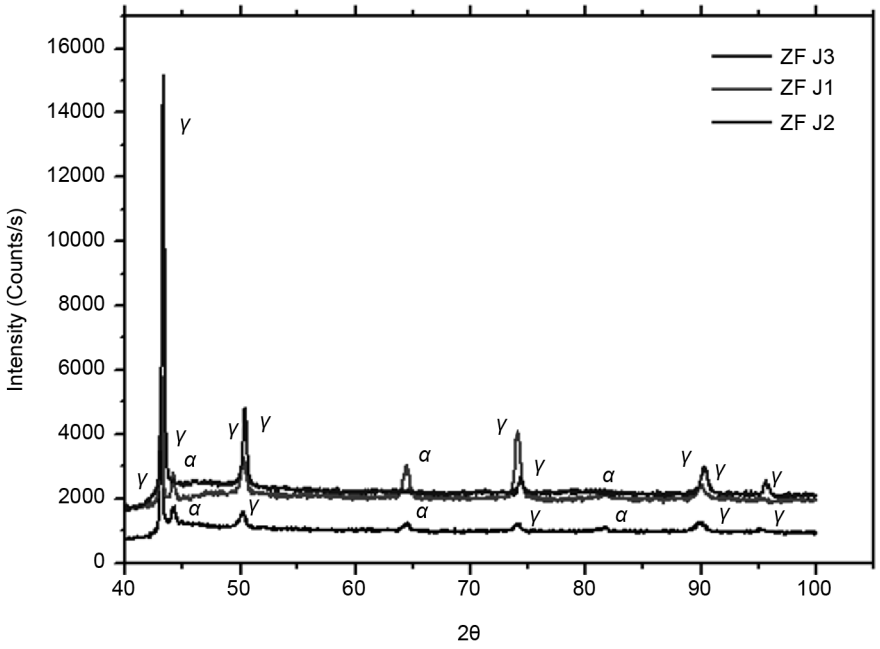

Figure 4. Standard X-ray diffraction on MZ-HAZ-MB regions of the super-duplex stainless steel welded joints.

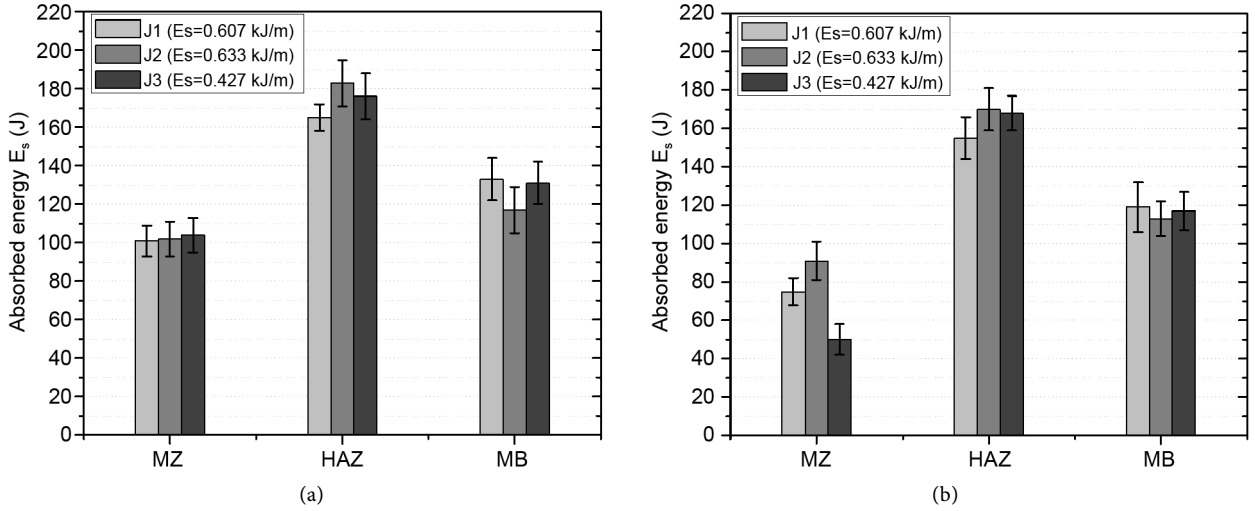

Figure 5. Average absorbed energy by the material during the impact tests on the regions of MZ-HAZ-MB in the conditions of (a) 25˚ and (b) −40˚C.

with high toughness resulting from small grain size on the HAZ and higher concentration of γ-phase which can prevent the propagation of cleavage cracks originating in the α-phase [30] [31]. Moreover, when the welding temperature is higher, the impact energy absorbed by both MZ and MB increases.

The higher toughness value in the HAZ compared to the one on the MB is normal in super-duplex steels due to the existence of the both phases (α and γ) present in the matrix. These two phases together provide good elastic and plastic behaviors which reflect the excellent levels of absorbed energy within the three regions. Additionally, for a smaller interpass temperature in the joint, a higher

toughness obtained. This was due to the robotic welding process, which contributes to a smooth metal transference without any distortion.

It is also worth bearing in mind that the microstructures after welding depend on the cooling rate. When there is high localized heat input, this affects the HAZ configuration (*i.e.* size and the region which will be formed). On the other hand, phases and morphologies arising in each region are results of the cooling conditions of the joints, due to the interpass temperature applied here, which was 40˚C. In multi-pass welding process occurs a kind of overlapping thermal cycles causing heating and reheating which provokes much more formation of austenite phase. This happens especially on the first weld bead contributing in this way for the increase of the toughness in the HAZ.

The toughness in the MB region is within an expected range for lower energies at a lower temperature of −40˚C. This result is acceptable since the transition temperature for SAF 2507 steel is −50˚C. In other words, the mechanical behavior of this region according to the small variation of absorbed energy is in agreement with the expected range for the α/γ phase ratio. The small variation in absorbed energies was a consequence of the local temperature gradient.

The impact tests at −40˚C showed a decrease in the toughness with some change in the structure of the α-phase when compared with data at room temperature. This behavior is associated with a great amount of γ-phase in the HAZ region which significantly reduces toughness, approximately by half, when the MZ region is evaluated. Furthermore, toughness decreasing at −40˚C is also related to the increase in the concentration of α-phase, and possibly the presence of precipitates of chromium nitride (Cr_2N), which generates a fragile microstructure with coalescence in the ferrite grains, creating residual stresses and increasing the γ-phase [30] [32]. It is seen that there is an increase in phase grain size and a reduction of the number of grains when the impact resistance is reduced.

Temperature variations modify the original microstructure, change the phase balance and, consequently, affect the joint performance. Repeated reheating on molten zone (MZ) and heated affected zone (HAZ) may lead to precipitation of secondary austenite and intermetallic phases [32]. Thermal cycles during welding process due to little controlled heating and cooling, can generate gradients of temperature that modify the balance of the austenite/ferrite phases. This can mainly occur during the reheating of the molten zone (MZ) and heated affected zone (HAZ) by forming precipitates of the sigma phase localized around the ferritic phase contours.

4.3. Pitting Corrosion Tests

Pitting corrosion tests were performed following the ASTM G48-A standard test method, with immersion in an acid solution for 24 hours at 22˚C. The values of mass loss per area were of 0.0308 g/cm^2 and 0.0353 g/cm^2 on J1 and J2 samples respectively. Note that the mass loss was higher than 0.0001 g/cm^2. This is an in-

dication of pits formation at the α/γ interface, consuming the interior of the ferrite grains, as shown in Figure 6. The mass loss on joint J3 was 0.0264 g/cm^2, the lower value being attributed to the lower welding energy.

EDS performed inside the pits, revealed also considerable amount of Mn, see point 4 on Figure 2. This suggests that nucleation and growth of these pitting occurs preferably in regions containing manganese sulfide (MnS) inclusions. As mentioned, this led to the formation of corrosion pitting at preferred sites, as well as on deformation bands of the α/γ-interface, generating discontinuity in the passive film. This is one of the reasons that contribute to fractures in steels when it is subjected to stress accompanied with microstructural changes and accumulated residual stresses. It is clear to see that the γ-phase presented less localized attacks (pitting) than the α-phase, and this is attributed to the Ni content in the γ-phase, which offers greater resistance to corrosion.

The estimated values of PREN for the three different welding energies, based on empirical equations reported in the literature are presented in Figure 7 [14] [15] [16] [28].

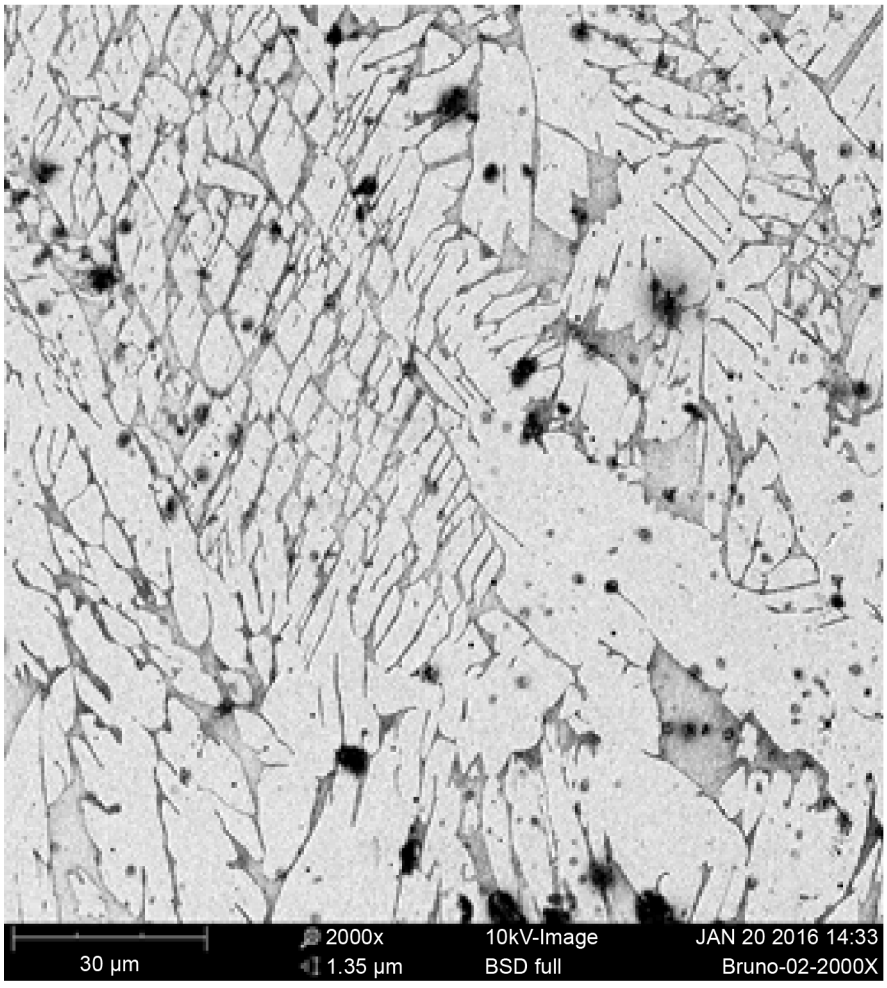

Figure 6. Pitting corrosion formed in the interior of the grain boundaries of the α-phase and precipitates σ-phase boundaries α/γ-phases.

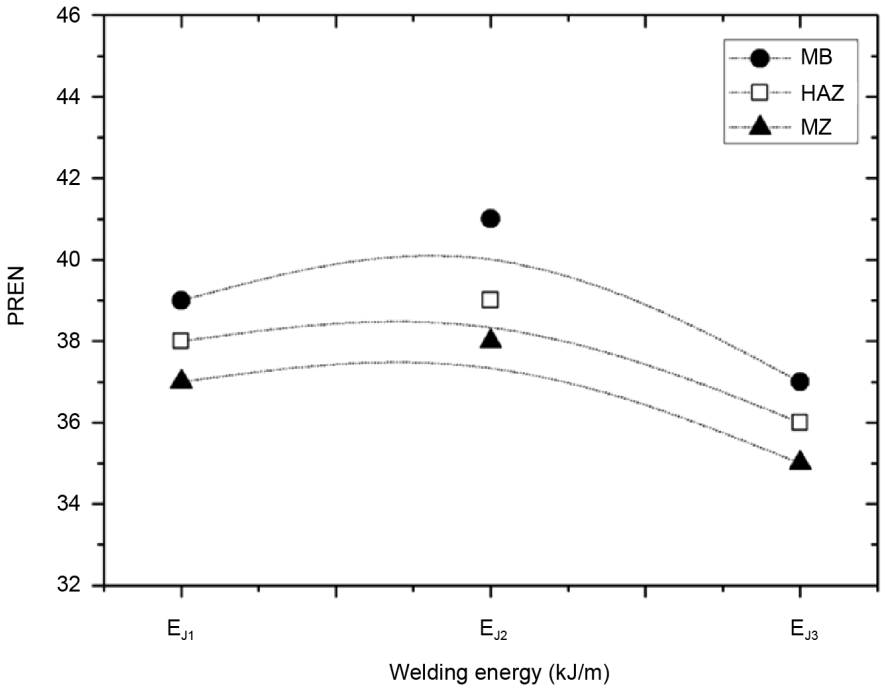

Figure 7. Correlation of PREN of the α/γ-phases related to the applied welding energies.

The coexistence of α/γ-phase modifies the estimated values of PREN affected more by the smaller phase. The calculated PREN values of the phases due to the partition of alloying elements were 41.66 (MB), 41.31 (MZ), 37.79 (α-phase) and 45.59 (γ-phase). The highest value in the γ-phase is associated with the higher welding energy applied, potentially due to the presence of alloying elements such as N. This element increases the toughness, resistance to pitting and work hardening rate and stabilizing the γ-phase.

It is worth mentioning here that N does not prevent the formation of σ-phase, but delays its formation, and its main function is the balance and increasing of δ/γ-ratio transformation rate [28] [33] [34]. Consequently, for higher value of PREN, the toughness and pitting corrosion resistance of the materials is improved. When the welding energy decreases, the difference of the δ/γ-ratio decreases as well, indicating a higher fraction of δ-phase, reducing the value of the PREN. This behavior is in agreement the calculated values for Cr(eq) = 29.5 and Ni(eq) = 15.4, which the HAZ and MZ regions as the most likely for the formation of corrosion pits (regions with lower content of Cr and Mo) according to the welding conditions.

4.4. Microhardness Tests

The microhardness tests were applied to the MB-HAZ-MZ region of the three joints, and the results are depicted in **Figure 8**. It is observed that the highest value of the microhardness occurred at the MZ region, average of 314 HV, while the lowest occurred at the MB region, average of 179 HV. The microhardness at the HAZ region was 248 HV. This proves that hardness was affected by the

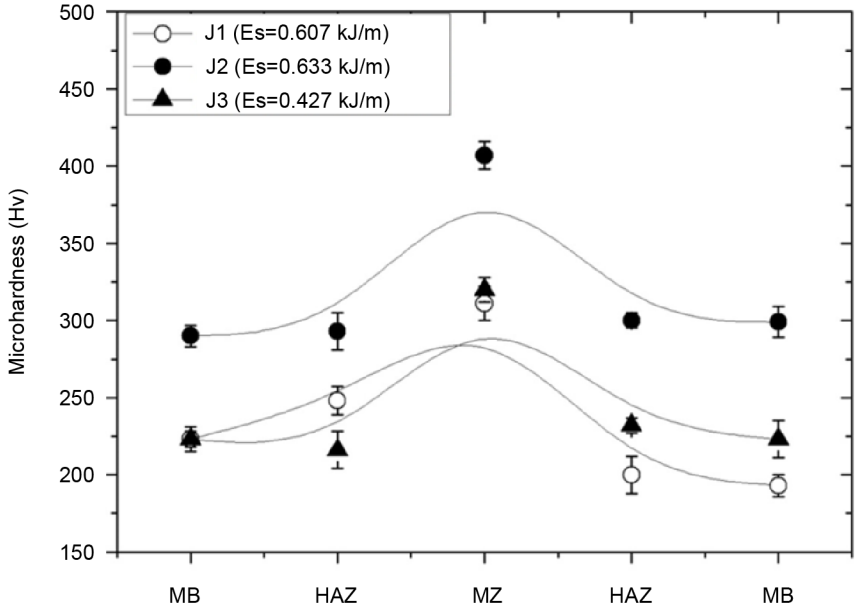

Figure 8. Microhardness profile on the welded joints in the regions of MZ-HAZ-MB for J1, J2 and J3.

thermal gradient on the welded joints. The welding promoted an increase of the microhardness on HAZ region with higher heat input. Moreover, the regions of higher microhardness were also the ones which present more γ-phase fraction due to higher amount of N and Ni, as seen in **Figure 2**.

The measured microhardness gradient on J2 showed to be higher when compared with the J1 with values of 290 HV (MB), 293 HV (HAZ) and 407 HV (MZ) obtained across the joint. The J3 presented lower hardness values as well as better austenite/ferrite energetic balance. This behavior was due to the lower welding energy applied here. The highest value for the MZ reflects the lower toughness of this region compared to HAZ and MB. Finally, J3 presented an average value equal to the MB in comparison with the other joints (223 HV), but showed lower microhardness on the HAZ, around 216 HV, as well as at the MZ with a microhardness of 311 HV. It is noticeable that when high levels of welding energy are applied, it contributes to increase the microhardness, but there is a reduction of these values when the direction MZ-HAZ-MB is evaluated. Note that at both the MZ (407 HV) and on HAZ (362 HV), their central position had higher microhardness, as shown in **Table 2**.

The MZ and HAZ regions presented higher values of microhardness than the MB region, though the microhardness in the HAZ varied, with a tendency to decrease as it approaches the MB. Due to that, there was a decrease in the toughness and pitting corrosion resistance as consequence of grain growth and the presence of ferrite under coalescence, reducing the hardening effect [26]. The microhardness difference in the HAZ is attributed to the different morphologies of α/γ-phases and the distribution of the σ-phase. The microhardness tests showed that the mechanical resistance of MZ region is greater than the MB.

This behavior is the related to N presence in solid solution, austenitic grain refinement and hardening through the effect of precipitates on σ-phase. Furthermore, as consequence of retained austenite in ferrite grain boundaries, recrystallization is limited and the occurrence of fine grains is favored, contributing to increase the resistance of the welded region.

4.5. SEM Aspects Associated with the Phase Diagram

The BSE-SEM analysis on the region where it was observed via EDS that changes in composition in the fraction of the α/γ-phases during the welding process occurred is shown in Figure 9. The presence of σ-phase in the ferrite grain boundaries formed with greater diffusion of Cr and precipitated colonies of chromium nitride (Cr_2N) in the contours of α-phase, in the α/y interface and at triple points. This is a product of the thermal cycle imposed during the welding process which deteriorated the toughness, microhardness and pitting corrosion resistance with a lower PREN [21] [35].

Table 2. Microhardness behavior along the three regions with different welding energies and phase fractions.

Welding energy (kJ/mm)	Microhardness (Hv) and fraction of phases (%)			
	Zone	Hv	α	γ
EJ1 = 0.607	MB	223	50 ± 5	50 ± 5
	HAZ	248	63 ± 7	37 ± 7
	MZ	314	38 ± 3	62 ± 3
EJ2 = 0.633	MB	290	50 ± 5	50 ± 5
	HAZ	293	68 ± 6	32 ± 6
	MZ	407	37 ± 4	63 ± 4
EJ3 = 0.427	MB	223	50 ± 5	50 ± 5
	HAZ	216	56 ± 4	44 ± 6
	MZ	314	44 ± 4	56 ± 4

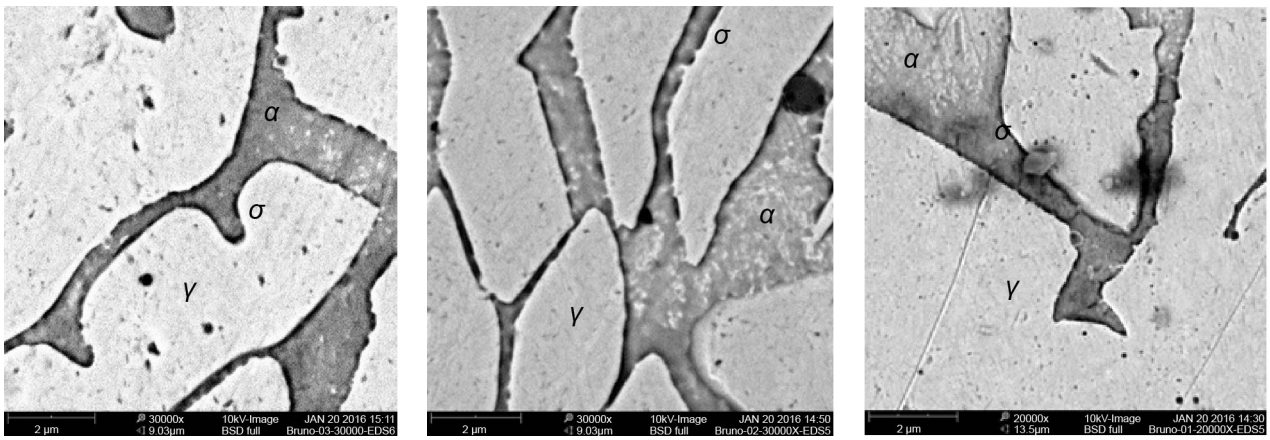

Figure 9. BSE-SEM image of σ-phase formation in α-phase grain boundaries of the α/γ-phase HAZ region.

Note that those results are consistent with the equilibrium phase diagram calculated by the Facstage software which also predicted the formation of following phases: α-phase, γ-phase, σ-phase, Cr_2N and $M_{23}C_6$ as shown in **Figure 10**. Although the phase diagram is calculated for a non-dynamic situation, the results here allowed to predict the possible phases formed in a temperature range in which the welding process was applied.

It is seen that in MZ, the amount of γ-phase is greater than in HAZ and MB with the presence of precipitated σ-phase in the ferritic grain boundaries in small fractions that can cause cracking by localized corrosion. This is an indication that the formation of σ-phase should be avoided during cooling and solidification because it reduces sharply the toughness of the material. The σ-phase removes and consumes Cr, Mo and N, reducing the PREN on adjacent regions, mainly in MZ region with lower welding energies [26] [31] [32].

5. Conclusions

The relationship between the pitting resistance equivalent numbers (*i.e.* pitting corrosion resistance), impact resistance and microhardness from the phases presented in the super-duplex SAF 2507 steel under welding parameters was investigated. Some crucial points should be addressed:

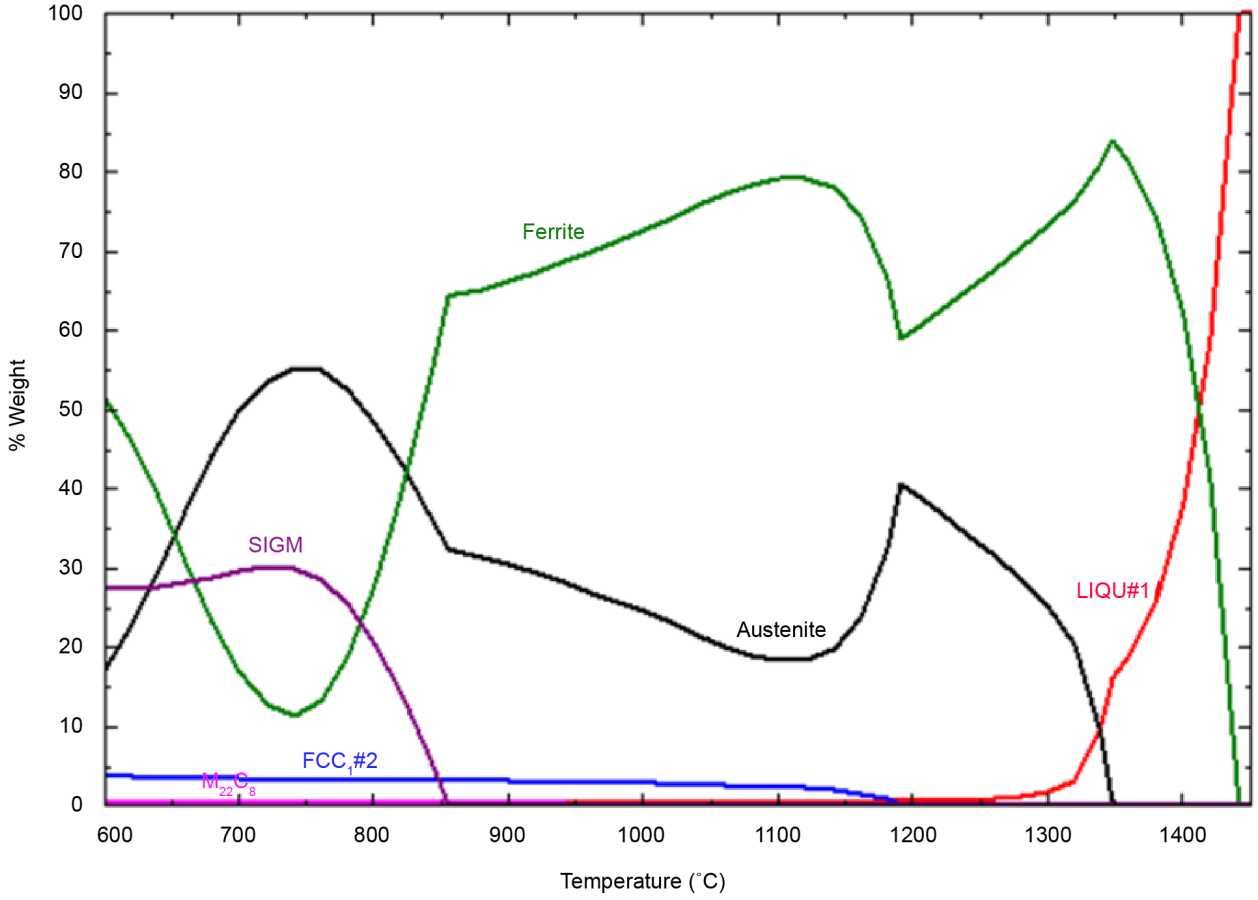

Figure 10. Equilibrium phase diagram of the material as a function of temperature.

1) The microstructures showed the presence of α/γ-phases in intergranular, Widmanstätten and allotriomorphic morphologies. Moreover, some occasional formation of σ-phase in the grain boundaries, preferably α/γ interfaces, and grain growth of the ferrite phase was observed.

2) Welding energy caused changes in the amount and transformation rate of α/γ-phases of the SAF 2507 steel. This affected the microhardness and toughness in the MZ-HAZ-MB regions with an increase in the amount of γ-phase in MZ and decrease of α-phase with higher welding energies.

3) The HAZ and MB showed good toughness at room temperature and also at low temperature (−40˚C) for different welding energies. However, the toughness at the MZ decreased significantly, even with the formation of γ-phase, due to ferrite grains coalesced and formation of σ-phase.

4) The welding applied on the SAF 2507 steel exhibited high value of microhardness in the HAZ and MB, due to the higher concentration of γ-phase. These elevated levels of microhardness in the HAZ are most probably due to the formation of σ-phase precipitates in the ferrite grain boundaries under low welding energies.

5) The pitting corrosion analysis showed greater mass loss for higher welding energy with pit formation on the α/γ interface surrounded by α-phase. The values of PREN, due to partition of the elements, modified the coexistence of α/γ-phases, and value of the PREN (γ) higher than the PREN (α) when the welding energy was higher.

Acknowledgements

The authors are in debit with Brazilian research funding agencies FAPEMA (Maranhão Foundation for Scientific Research and Development), CNPq and CAPES. They would also like to acknowledge Prof. Regina Célia (UFMA) and Mr. José Renato Sucupira for technical supports and Prof. In-Ho Jung from McGill University for providing access to FactSage thermodynamic software.

References

[1] Solomon, H.D. and Koch, E.F. (1979) High Temperature Precipitation of α' in a Multicomponent Duplex Stainless Steel. *Scripta Metallurgica*, **10**, 971-974. https://doi.org/10.1016/0036-9748(79)90331-4

[2] Baeslack, W. and Lippold, J.C. (1988) Phase Transformation Behavior in Duplex Stainless Steels Weldments. *Metal Construction*, **20**, 26-31.

[3] Charles, J. (1991) Super Duplex Stainless Steels: Structure and Properties. *Duplex Stainless Steels*'91, Les Editions de Physique, Vol. 1, Les Ulis Cedex, France.

[4] Chail, G. and Kangas, P. (2016) Super and Hyper Duplex Stainless Steels: Structures, Properties and Applications. *Procedia Structural Integrity*, **2**, 1755-1762. https://doi.org/10.1016/j.prostr.2016.06.221

[5] Davison, R.M. and Redmond, J.D. (1991) A Guide to Using Duplex Stainless Steels. *Materials & Design*, **12**, 187-192. https://doi.org/10.1016/0261-3069(91)90162-W

[6] Rauta, R.P., Rodrigues, S.F., Leal, V.S., Reis, G.S., Aranas Jr., C. and Ferraresi, V.A. (2016) Influence of Pushing and Pulling the Electrode Procedure and Addition of

Second Layer of Welding on the Wear in Hardfacing of Fe-Cr-C. *Materials Research*, **19**, 1193-1200. https://doi.org/10.1590/1980-5373-MR-2016-0230

[7] Brandi, S.D. (2003) Some Aspects of Weldability and Jointability of Duplex Stainless Steels. *Materials Science Forum*, **426-432**, 4063-4068. https://doi.org/10.4028/www.scientific.net/MSF.426-432.4063

[8] Garfias-Mesias, L.F., Syke, J.M. and Tuck, C.D.S. (1996) The Effect of Phase Compositions on the Pitting Corrosion of 25 Cr Duplex Stainless Steel in Chloride Solutions. *Corrosion Science*, **38**, 1319-1330. https://doi.org/10.1016/0010-938X(96)00022-4

[9] Syed, R., Jiang, W., Wang, C. and Iqbal Sabir, M. (2015) Fatigue Life of Stainless Steel 304 Enhancement by Addition of Multi-Walled Carbon Nanotubes (MWCNTs). *Journal of Mechanical Science and Technology*, **29**, 291-296. https://doi.org/10.1007/s12206-014-1235-7

[10] Kobayashi, D.Y. and Wolynec, S. (1999) Evaluation of the Low Corrosion Resistant Phase Formed during the Sigma Phase Precipitation in Duplex Stainless Steels. *Materials Research*, **2**, 239-247. https://doi.org/10.1590/S1516-14391999000400002

[11] Lee, K.M., Cho, H.S. and Choi, D.C. (1999) Effect of Isothermal Treatment of SAF 22005 Duplex Stainless Steel on Migration of δ/γ Interface Boundary and Growth of Austenite. *Journal of Alloys and Compounds*, **285**, 156-161. https://doi.org/10.1016/S0925-8388(99)00014-6

[12] Ramirez, A.J., Lippod, J.C. and Brandi, S.D. (2003) The Relationship between Chromium Nitride and Secondary Austenite Precipitation in Duplex Stainless Steels. *Metallurgical and Materials Transactions*, **43A**, 1575-1597. https://doi.org/10.1007/s11661-003-0304-9

[13] Gunn, R.N. (2003) Duplex Stainless Steels. Microstructure, Properties and Applications. Abington Publishing, Cambridge, 204.

[14] Magnabosco, R. and Alonso-Falleiros, N. (2005) Pit Morphology and Its Relation to Microstructure of 850˚C Aged Duplex Stainless Steel. *Corrosion*, **61**, 130-136. https://doi.org/10.5006/1.3278167

[15] Jia, D.B., Dai, W.B., Tang, G.P., Xu, C.Z., Tian, X.Z. and Yu, K.J. (2017) Improvement of Pitting Corrosion Resistance of Stainless Steel by Electric Current Pulse. *Materials Science and Technology*, **33**, 1417-1420. https://doi.org/10.1080/02670836.2016.1277092

[16] Sato, Y.S., Nelson, T.W., Sterling, C.J., Steel, R.J. and Pettersson, C.O. (2005) Microstructure and Mechanical Properties of Friction Stir Welded SAF 2507 Super Duplex Stainless Steel. *Materials Science and Engineering A*, **395**, 376-384. https://doi.org/10.1016/j.msea.2005.02.054

[17] Gideon, B., Ward, L. and Biddle, G. (2008) Duplex Stainless Steel Welds and Their Susceptibility to Intergranular Corrosion. *Journal of Minerals & Materials Characterization & Engineering*, **7**, 247-263. https://doi.org/10.4236/jmmce.2008.73019

[18] Wang, J., Lu, M., Zhang, L., Chang, W., Xu, L. and Hu, L. (2012) Effect of Welding Process on the Microstructure and Properties of Dissimilar Weld Joints between Low Alloy Steel and Duplex Stainless Steel. *International Journal of Minerals, Metallurgy and Materials*, **19**, 518-524. https://doi.org/10.1007/s12613-012-0589-z

[19] Ghosh, S.K. and Mondal, S. (2008) High Temperature Ageing Behavior of a Duplex Stainless Steel. *Materials Characterization*, **59**, 1776-1783. https://doi.org/10.1016/j.matchar.2008.04.008

[20] Pohl, M., Stoz, O. and Glogowski, T. (2007) Effect of Intermetallic Precipitations on the Properties of Duplex Stainless Steels. *Materials Characterization*, **58**, 65-71.

https://doi.org/10.1016/j.matchar.2006.03.015

[21] Badji, R., Bouabdallah, M., Bacroix, B., Kahloun, C., Belkessa, B. and Maza, H. (2008) Phase Transformation and Mechanical Behavior in Annealed 2205 Duplex Stainless Steel Welds. *Materials Characterization*, **59**, 447-453. https://doi.org/10.1016/j.matchar.2007.03.004

[22] Brandi, S.D., Silveira, L.M.Y. and Vasconcellos, D.L.B. (2010) Aplicacao da norma ASTM A923-Pratica A para identificacao de fases intermetalicas em junta soldada de aco inoxidavel superduplex UNS 32750. *Revista Escola de Minas*, **61**, 153-158. https://doi.org/10.1590/S0370-44672010000100026

[23] ASTM E-23-05 (2005) Standard Test Methods for Notched Bar Impact Testing of Metallic Materials. ASTM, West Conshohocken.

[24] ASTM G 48-00 (2000) Standard Test Methods for Pitting and Crevice Corrosion Resistance of Stainless Steel and Related Alloys by Use of Ferric Chloride Solution. ASTM, West Conshohocken.

[25] Nascimento, C.C.F., Rodrigues, S.F., Morais, V.M. and Vilarinho, L.O. (2016) Methodology for Corrosion Evaluation in HAZ of 11%-Cr Ferritic Stainless Steel. *Journal of Mechanical Science and Technology*, **30**, 3805-3811. https://doi.org/10.1007/s12206-016-0743-z

[26] Mohammed Asif, A., Shrikrishna, K.A., Sathiya, S. and Goel, S. (2015) The Impact of Heat Input on the Strength, Toughness, Microhardness, Microstructure and Corrosion Aspects of Friction Welded Duplex Stainless Steel Joints. *Journal of Manufacturing Processes*, **18**, 92-106. https://doi.org/10.1016/j.jmapro.2015.01.004

[27] Santos, T.F.A., Marinho, R.R., Paes, M.T.P. and Ramirez, A.J. (2013) Microstructure Evaluation of UNS S32205 Duplex Stainless Steel Friction Stir Welds. *Revista Escola de Minas*, **66**, 187-191. https://doi.org/10.1590/S0370-44672013000200008

[28] Ha, H.Y., Jang, M.H., Lee, T.H. and Moon, J. (2014) Interpretation of the Relation between Ferrite Fraction and Pitting Corrosion Resistance of Commercial 2205 Duplex Stainless Steel. *Corrosion Science*, **89**, 154-162. https://doi.org/10.1016/j.corsci.2014.08.021

[29] Ha, H.Y., Jang, M.H., Lee, T.H. and Moon, J. (2015) Understand the Relationship between Phase Fraction and Pitting Corrosion Resistance of UNS S32750 Stainless Steel. *Materials Characterization*, **106**, 338-345. https://doi.org/10.1016/j.matchar.2015.06.019

[30] Hong, J., Han, D., Tan, H., Li, J. and Jiang, Y. (2013) Evaluation of Aged Duplex Stainless Steel UNS S32750 Susceptibility to Intergranular Corrosion by Optimized Double Loop Electro-Chemical Potentiokinetic Reactivation Method. *Corrosion Science*, **68**, 249-255. https://doi.org/10.1016/j.corsci.2012.11.024

[31] Lippold, J.C. and Kotecki, D.J. (2005) Welding Metallurgy and Weldability of Stainless Steels. Wiley, Hoboken.

[32] Maetz, J.Y., Douillard, T., Cazottes, S., Verdu, C. and Kleber, X. (2016) M23C6 Carbides and Cr_2N Nitrides in Aged Duplex Stainless Steel: A SEM, TEM and FIB Tomography Investigation. *Micron*, **84**, 43-53. https://doi.org/10.1016/j.micron.2016.01.007

[33] Ramkumar, K.D., Thiruvengatam, G., Sudharsan, S.P., Mishra, A. and Sridhar, R. (2015) Effect of Optimal Weld Parameters in the Microstructure and Mechanical Properties of Autogenous Gas Tungsten Arc Weldments of Super-Duplex Stainless Steel UNS S32750. *Materials and Design*, **66**, 356-365. https://doi.org/10.1016/j.matdes.2014.10.084

[34] Chehuan, T., Dreilich, V., Kioshy, S.A. and Mattos, O.R. (2014) Influence of Multi-

pass Welding on the Corrosion Resistance of a Superduplex Stainless Steel Subjected to Pulsed Gas Metal Arc Welding. *Corrosion Science*, **86**, 268-274. https://doi.org/10.1016/j.corsci.2014.06.004

[35] Ma, M., Ding, H., Tang, Z., Zhao, J., Jiang, Z. and Fan, G. (2016) Effects of Temperature and Strain Rate on Flow Behavior and Microstructural Evolution of Super Duplex Stainless Steel under Hot Deformation. *Journal of Iron and Steel Research International*, **23**, 244-252. https://doi.org/10.1016/S1006-706X(16)30041-3